THE EFFECT OF GEOMETRY ON THE GAS DYNAMICS IN AVALANCHE CONTROL GAS EXPLODERS INTERNATIONAL SNOW SCIENCE WORKSHOP 2026, WHISTLER, CANADA

Kevin Cheevers[1], Logan Maley[2], Elizabeth Ramey[1], Matei Radulescu[*1]

[1] *University of Ottawa, Ottawa, ON. Canada*
[2] *Okanagan College - Kelowna Campus, Kelowna, BC, Canada*

ABSTRACT: The avalanche control industry is shifting towards the Remote Avalanche Control Systems (RACS) to protect both public and private infrastructure such as ski areas and transportation corridors. Though these systems originally employed condensed phase (solid) explosives, over recent decades, detonation tubes, also known as gas exploders in the snow community, have become increasingly popular. Currently, the bulk of the research into RACS has been conducted for solid point-source explosives. The growing popularity and prevalence of gas exploders in the field have led to an increase into gas RACS research. From experimental and field pressure measurements on the snowpack, it has been shown that spherical expansion of solid point-source explosions develop different pressure profiles compared to the directional blast waves of gas exploders. There remains a lack of clarity regarding the gas dynamics leading to the observed pressure waves above the snowpack.

In this study, we characterize the dynamics of the shock wave driven by a gas exploder through state-of-the-art numerical simulations and provide a closed form analytical solution that identifies the relevant parameters and scaling laws. The model developed was found in excellent agreement with simulations. The dynamics of the air blast wave established by the detonation tube is shown to consist primarily in a layer of compressed air, driven by the momentum transfer from the combustion products exiting the tube and the slowing down effect of air accumulation in the geometrically growing layer. Calculations of reflection of the compressed air layer with a reflective surface clarifies the momentum transfer mechanism involving the re-direction of momentum as the jet impacts the ground and gets re-directed.

KEYWORDS: Remote Avalanche Control Systems, Gas Dynamics, Shock Dynamics, CFD

1. INTRODUCTION

Avalanches are one of the most persistent natural hazards affecting transportation corridors, ski and recreation areas, mining operations and communities in mountain regions during the winter season. Stakeholders, such as communities, governments and companies, have been working to improve the preventative approach to avalanches through installation of infrastructure (snow fences, avalanche sheds, etc.), as well as artificial triggering of avalanches before the snow volume builds to a dangerous level. Currently, this artificial triggering is done in several ways, hand thrown bombs (from skiers or helicopters), use of artillery, and Remote Avalanche Control Systems (RACS).

The modern development of RACS offers significant safety improvements over other explosive delivery systems, as it does not expose humans as much to the inherent explosive or avalanche hazards. Currently operating RACS generally fall into two categories: remote deployable bombs, such as Wyssen and North American Avalanche Guard System as well as gas exploders such as Gazex, DaisyBell, and O'Bellx. Both types of systems use a shock wave produced above the snow to impact and trigger an avalanche. The shock waves differ in their configuration if they are produced by a point-source or in a detonation tube.

Decades of experimental research work has been conducted studying how blast waves impacting the snow can trigger avalanches (Perla 1976; Gubler 1977; Lachapelle 1977; Simioni et al. 2017; Simioni and Schweizer 2018; Larson et al. 2022; Meier 2024). Much of the work has been done for condensed phase explosives expanding from a pseudo point source (Gubler 1977; Friedlander 1946; Brown 1980). In recent years, the popularity of gas exploders has grown and work has been done to characterize and predict the blast wave profiles produced from the detonation of gas in a tube (Meier 2024; Seitz 2021; Simioni et al. 2017; Larson et al. 2022).

Modern numerical modelling work has been conducted to improve the understanding of how various parameters affect the way in which air blasts from either point source or detonation tubes trigger avalanches. Work done by Miller et al. (2010) and

* *Corresponding author address:*
Matei Radulescu, University of Ottawa,
Ottawa, Canada K1N 6N5;
tel: +1 613-878-4150
email: matei@uottawa.ca

https://doi.org/10.15788/1790098812

Miller et al. (2011) simulated both the air space and snow space affected by a blast wave and captured the nonlinear response of a shock impacting the snow. A model produced by Sidler (2015) was developed to better predict the snow response to a blast wave for porous material. This model was shown to be better than viscoelastic continuum models and the work was extended to compare the model to acoustic field measurements (Sidler et al. 2016). Generally, recent work shows a departure from empirically driven work, though significant work remains to develop a systematic understanding of the specific mechanisms at play (i.e. installation geometry, tube geometry and gas mixture).

Detonation tubes are also known as *pulse-detonation engines* in the aerospace field of research, where repeated operation provides a thrust-producing device. Despite their extensive development for propulsion applications, there is currently no existing model to predict the pressure decay from their exhaust in air. Existing models are empirical fits to experimental data borrowing scaling laws from the point-source blast wave scaling (Anand et al. 2018).

In the current study, we conduct detailed simulations focusing on the detonation tube exit to clarify the dynamics affecting the blast wave driven by the exhaust of detonation products. An analytical model is formulated to produce a simplified prediction of the evolution of the shock strength as the blast wave travels into the far-field where it can impact the snow surface. To complement the model, numerical simulations have also been conducted to show how the transmitted blast wave impacts the snow surface and what forces are generated on a rigid snow surface.

2. PHYSICAL MODEL & NUMERICAL METHOD

We first computed the solution to the problem of a blast wave exiting an infinitely long cylindrical tube into ambient air. The problem is modeled using the two-dimensional axisymmetric Euler equations using the perfect gas equation of state. All variables are non-dimensionalized using the ambient air density ρ_0, pressure p_0, and tube diameter D. A constant ratio of specific heats $\gamma = 1.4$ is enforced across the entire domain to capture the dynamics of the ambient air outside the tube.

The detonation wave exiting the tube is modelled by initializing the gas within the tube to the Chapman–Jouguet (CJ) state calculated for a stoichiometric octane–oxygen mixture. The CJ density ρ_{CJ}, flow velocity u_{CJ}, and speed of sound c_{CJ} are directly mapped onto the interior tube domain. While enforcing $\gamma = 1.4$ introduces a minor discrepancy in the static CJ pressure, matching these primitive properties accurately recovers both the acoustic impedance ($\rho_{\mathrm{CJ}} c_{\mathrm{CJ}}$) governing the wave transmission at the exit interface and the exiting momentum flux ($\rho_{\mathrm{CJ}} u_{\mathrm{CJ}}$), which reproduces the effective piston motion driving the shock through ambient air. Initial gas properties are summarized in Table 1.

Table 1: Initial conditions.

Property	Ambient Air	Detonation Products (CJ)
$\boldsymbol{\rho}^*$	1.0	2.428
$\boldsymbol{u}^*$	0.0	3.711
$\boldsymbol{v}^*$	0.0	0.0
$\boldsymbol{p}^*$	1.0	32.4

The governing equations are solved in cylindrical coordinates using a nominally second-order exact Riemann solver with Adaptive Mesh Refinement (Falle et al. 1993). Spatial resolution dynamically scales from a base grid of 10 cells/diameter up to a maximum resolution of 160 cells/diameter. The central axis at $r = 0$ is assigned an axisymmetric symmetry boundary condition, while all outer domain boundaries employ zero-gradient outflow conditions. Solid tube walls are modelled using rigid reflecting boundary conditions.

3. SIMULATION RESULTS

The non-dimensional pressure and density contours are presented in Figure 1. As the detonation wave exits from the tube into ambient air, the initial interface interaction forms a Riemann problem consisting of a transmitted lead shock, a right-propagating contact surface, and a reflected expansion wave travelling back into the tube, driven by the higher density of the detonation products relative to ambient air. As the wave exits the confinement, it diffracts around the tube end, transforming the initially planar transmitted shock into a quasi-spherical profile. A centered expansion wave originating at the corner communicates this sudden geometric expansion to the flow field. In the initial frame ($\tilde{t} = 0.745$), the exiting flow undergoes a rapid geometrically driven expansion analogous to expanding into a near-vacuum. The high-velocity displacement of ambient air by the expanding driver gas sustains the primary lead shock front. To match the low pressure of the over-expanded driver gas with the higher pressure be-

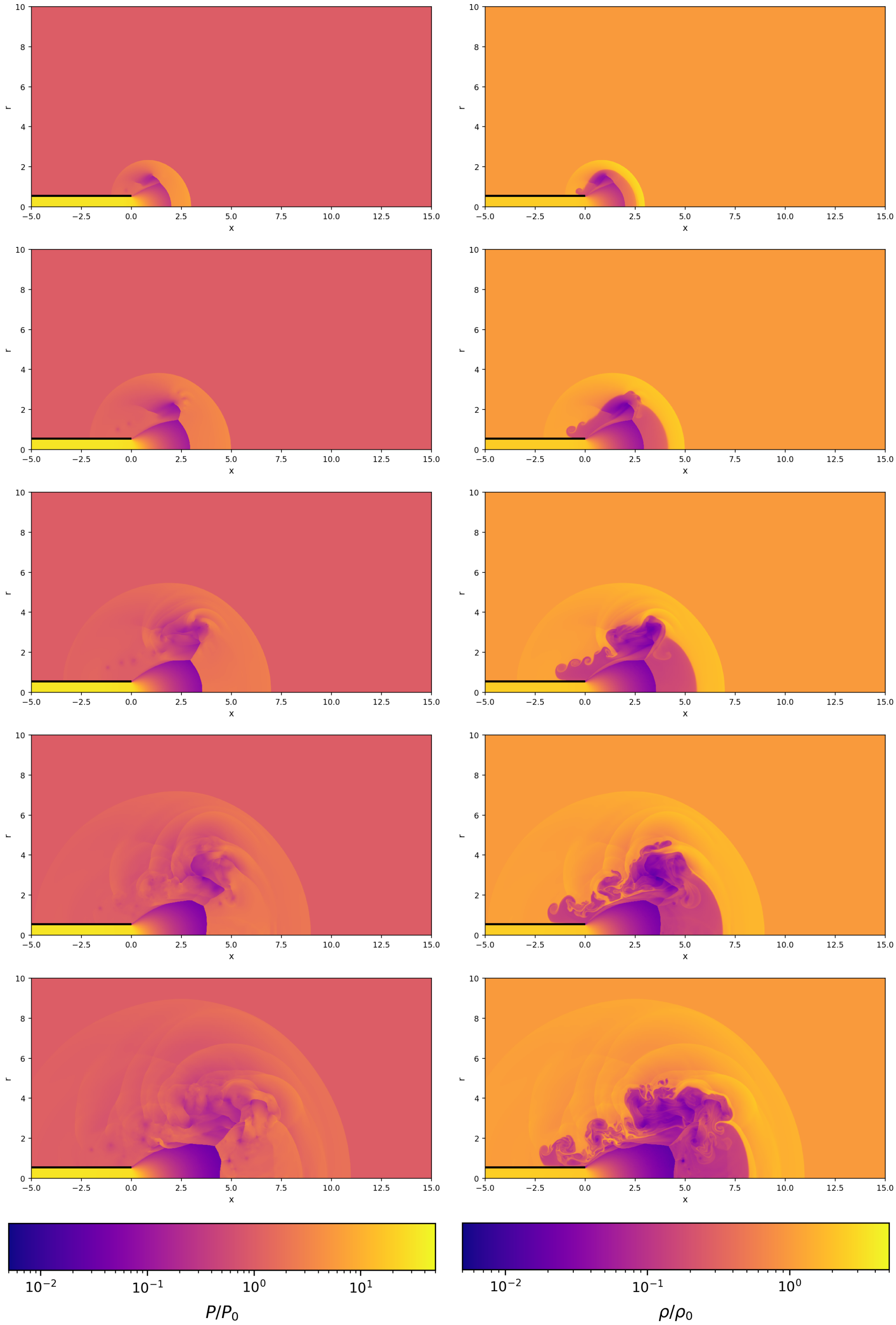

Figure 1: Contour Plots of (left) pressure, and (right) density, at time $t = 0.745$, 1.540, 2.540, 3.670, 4.905.

hind the lead shock, an internal, rear-facing shock forms. This shock re-compresses the expanded product gases, establishing a region of nearly uniform pressure behind the lead wave. The contact surface separating the detonation products from the ambient air is visible in the density field, situated between the lead shock and the rear-facing shock.

In the subsequent frames ($\tilde{t} = 1.540$ and 2.540), the quasi-spherical blast structure continues to expand outward as the lead shock front progressively decays. This decay is accompanied by an increase in the distance separating the lead and rear-facing shocks from the contact surface. The flow exiting the tube can also be seen to expand to a lower pressure and density as the rear-facing shock distances itself from the tube exit. The two final frames ($\tilde{t} = 3.670$ and 4.905) show a further decay in the blast wave accompanied by a further increase in the separation distances. However, the rear-facing shock begins to stabilize towards a fixed distance from the tube exit, breaking the spherical symmetry observed at earlier times.

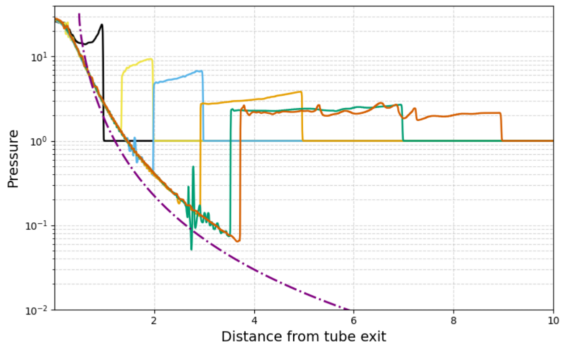

Figure 2: Pressure Profile along the central axis. Dash-dotted line from steady 1-dimensional theory.

The pressure profile along the central axis is presented in Figure 2. In the near field of the tube ($x \leq 1$), the lead shock retains its square wave profile with minimal expansion of the flow. As the shock distances itself from the tube ($x \geq 1$), the spatial profile consists of the expansion of the flow exiting the tube which follows a common curve due to the isentropic nature of the expansion. This is followed by an increase in pressure across the rear facing shock. The high pressure region between the two shocks has a shallow pressure gradient which decays in time. Eventually, the multidimensional nature of the phenomenon appears through the form of fluctuations, appearing once the lead shock has propagated sufficiently far from the tube exit ($x \geq 9$). These pressure fluctuations appear from the pressure waves generated in the mixing regions having propagated inwards towards the axis.

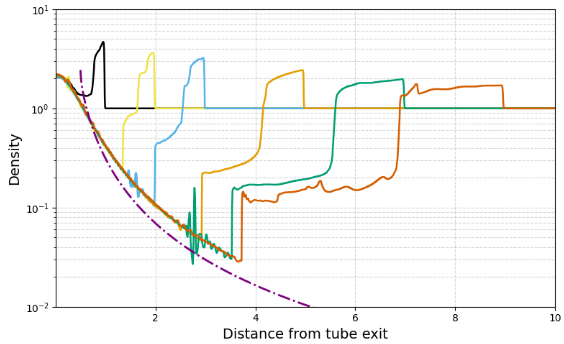

Figure 3: Density Profile along the central axis. Dash-dotted line from steady 1-dimensional theory.

The density profile is presented in Figure 3. Similar to the pressure profiles, the flow expansion at the exit of the tube follows a common curve due to the isentropic expansion process. The density disparity of the flow on both sides of the contact surface is evident in this figure, with the density of the products expanding to a density which is an order of magnitude smaller than the density of the shocked air.

4. ENGINEERING MODEL

We derived a closed form model for the dynamics of the leading shock wave. The leading shock is sustained by the detonation products, which act as a piston. The strategy is to establish first the dynamics of this interface (the piston). This will then permit to apply the shock jump conditions, which will provide the evolution of the shock pressure history as it decays from the tube exit.

The problem along the axis can be treated as a problem with spherical symmetry. At time 0, a spherical source turns on with flow density and speed denoted by ρ_s, u_s and source radius as $R_s = R_T$, where R_T is the tube exit radius. Upon the start of the source, the interface drives a lead shock (S1) and backward facing shock (S2), the expanding flow between the source and the backward facing shock is steady. We take a control volume bounding the material between the two shocks (see Figure 4). We assume that the material in this layer moves at the speed of the interface and has uniform properties at a given time, an assumption that is well supported by the simulations shown in the previous section. The conservation

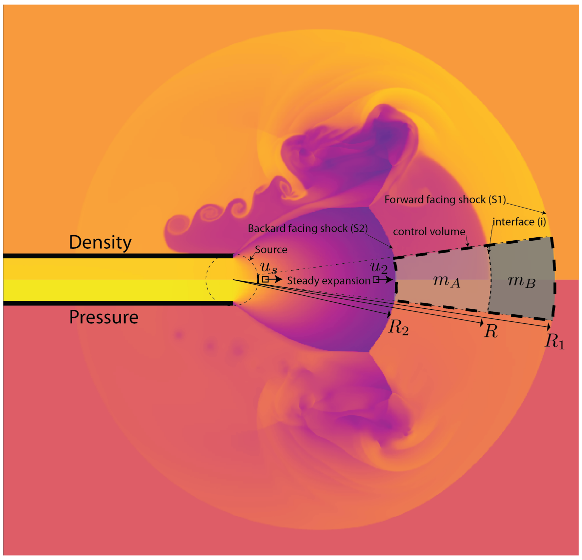

Figure 4: The model tracks the evolution of the material accumulating between the forward facing and backward facing shocks along the axis.

of linear momentum for this material yields

$$\frac{d}{dt}\left((m_A+m_B)\frac{dR}{dt}\right)=\dot{m}_s\left(u_2-\dot{R}_2\right)+p_2A_2-p_0A_1 \tag{1}$$

As we are interested in the dynamics of this gas for $R \gg R_S$, when the mass of the products shocked by the backward facing shock m_A is negligible compared with the mass of air driven by the interface m_B. As the gas in the steady region accelerates from u_s to u_2, the speed at which the backward facing shock $\dot{R}_2$ is propagating is negligibly small. As the flow in the expansion region accelerates to hypersonic speeds, the pressure p_2 is negligible compared to the momentum flux $\dot{m}_s u_2$. Likewise, the pressure of the ambient air is assumed to play a negligible role, as verified numerically a posteriori. The momentum balance simplifies to

$$\frac{d}{dt}\left(m_B\frac{dR}{dt}\right)=\dot{m}_s u_2 \tag{2}$$

The mass of the air can be approximated by

$$m_B=\rho_0\frac{4}{3}\pi\left(R_1^3-R_s^3\right)\cong\rho_0\frac{4}{3}\pi R^3 \tag{3}$$

while the mass flux exiting the source is

$$\dot{m}_s=4\pi R_s^2\rho_s u_s \tag{4}$$

We also take the speed of the gas in the steady expansion to be close to its maximum speed in a free hypersonic expansion as:

$$u_2=u_{max}=u_s\sqrt{\frac{\gamma_s-1+2/M_s^2}{\gamma_s-1}} \tag{5}$$

Where γ_s is the ratio of specific heats of the gas emanating from the source. Integrating the ODE with initial conditions at $t=0$, $R=R_s\to 0$ and $dR/dt=u_{max}$ provides the evolution of the interface radius with time $R(t)$. This relation can be differentiated to obtain the speed of the interface:

$$u_p(t)=\frac{dR}{dt}=\frac{\varphi}{R(t)}=\sqrt{\frac{\varphi}{2t}} \tag{6}$$

with

$$\varphi=\sqrt{\frac{3}{2}\frac{\rho_s}{\rho_0}u_s^2R_s^2\sqrt{\frac{\gamma_s-1+\frac{2}{M_s^2}}{\gamma-1}}} \tag{7}$$

Which shows that the piston speed decays as $\frac{1}{R}$ or as $\frac{1}{\sqrt{t}}$. Given the speed of the piston driving the lead shock, the shock overpressure is obtained from the Rankine-Hugoniot shock jump relations in terms of u.

$$z(t)\equiv\frac{p_{S1}-p_0}{p_0} \tag{8}$$

$$=\frac{\gamma(\gamma+1)}{4}\left(\frac{u_p}{c_0}\right)^2\left(1+\left(1+\left(\frac{\gamma+1}{4}\frac{u_p}{c_0}\right)^{-2}\right)^{\frac{1}{2}}\right) \tag{9}$$

The lead shock position can be expressed in terms of the piston position. Assuming the gas evolution between the piston and lead shock is in quasi-steady state, we can relate R_1 to R by the Rankine-Hugoniot relations:

$$\frac{R_1}{R}=\frac{D}{u}=\frac{\gamma+1}{2} \tag{10}$$

The resulting shock pressure is shown in Figure 5 along with the results of the numerical simulations. Very good agreement is obtained. This provides for the first time a closed form prediction of the shock pressure driven by a gas detonation tube, which can be used in engineering calculations for gas exploders.

Also shown in Fig. 5 is the prediction of the shock pressure without neglecting the speed of the control volume in (1) and accounting for the gas speed evolution $u_2(r)$. This requires the numerical integration of the following ODE

$$\frac{d}{dt}\left(m_B\frac{dR}{dt}\right)=\dot{m}_s\left(u_2-\dot{R}_2\right) \tag{11}$$

but provides excellent fidelity of the pressure evolution of the lead shock.

5. BLAST WAVE IMPINGING ON A SURFACE

To visualize how the expanding shock wave impacts the angled surface, two-dimensional simu-

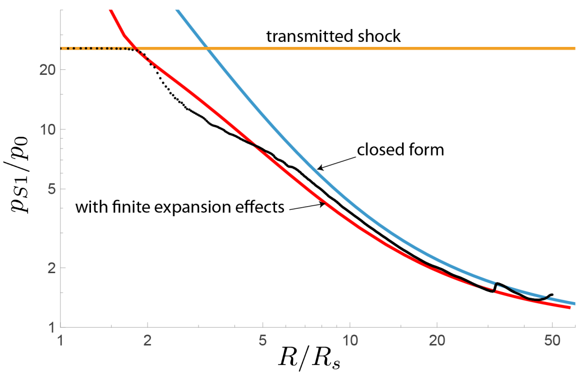

Figure 5: The shock pressure dependence on axial distance obtained numerically and analytically; blue line is the closed form solution given by (9) while the red line is the numerical integration of (11).

lations were done with OpenFoam using the RhoCentralFoam solver. The example presented in Figures 6 is set up with a horizontal shock tube and an angled surface set 40 degrees from the centerline of the shock tube as seen in Figure 6 A). The shock wave in this simulation is driven from a high-pressure gas (P = 633.592 kPa) suddenly released from the tube into 1 bar of pressure.

Figure 6 A shows the shock wave expanding out of the tube before impacting the surface. As the shock wave expands further, it first impacts the surface at point 1 which corresponds to the minimum distance from the exit of the tube to the surface. The shock wave forms a regular reflection which expands away from the surface while the incident shock wave continues to impact the surface. In figure 6 C the regular reflection has expanded and shows some distortion from interacting with the flow trailing behind the incident shock wave. As the shock continues to impact the surface, the reflection transitions to a Mach reflection which can be seen at point 4.

We can estimate the shear and normal forces on the surface assuming it is a rigid surface. The normal pressure on the surface can be estimated using the pressure in the first cell from the boundary. In these simulations the boundary layer was not resolved, the shear on the wall can be estimated from taking the velocity of the first cell from the wall as the free stream velocity and calculating the shear force with the empirical 1/7th power law. By integrating the forces for each time-step the impulse on the surface can be estimated for each cell. Figure 7 shows an estimate of the impulses from shear and normal pressure plotted as a distance along the surface from point 0. The plot is marked with ℄ to show the location of where the centerline of the tube meets the surface.

This shows that the point of highest normal impulse take place where the flow stagnates against the surface at point 2. This point is slightly further along the surface from where the initial shock impacts the surface, seen at point 1. Point 2 also shows the point where the shear force diverges. Before that point the shear force is in the negative direction (towards point 0) and after that the shear force is in the positive direction. The shear force steadily rises from point 2 until around point 4. After this point the normal force and shear force begin to reduce as the flow field dissipates. The normal force develops a second peak after the shock reflection transitions into a Mach reflection seen around point 4.

This gives an estimate of the behaviours seen on a rigid snow surface. The normal force is orders of magnitude larger than the shear force and has two peaks. The shear force shows a divergence where the snow would experience being pulled apart.

6. SUMMARY

This ongoing study seeks to clarify the gas dynamics and surface loading mechanisms of blast waves generated by gas-based RACS. Axisymmetric numerical simulations demonstrate the formation of a quasi-spherical structure comprised of a lead shock, followed by a contact surface separating detonation products from quiescent air. Behind this interface, a rear-facing shock recompresses the detonation products that undergo quasi-steady expansion upon exiting the tube. Modelling the evolution of this layer as a spherical piston driving a shock yields a closed-form analytical model in strong agreement with numerical results, providing a predictive blast decay model derived from first principles.

Simulations of the blast wave impinging on an angled wall reveal that normal impulse dominates shear impulse by orders of magnitude. The maximum normal force occurs at the flow stagnation, with a secondary peak emerging as the shock transitions from a normal reflection to a Mach reflection. The stagnation point is also the location where shear stress diverges, subjecting the surface to localized tension. Preliminary validating experiments will be presented at the conference, with future work to study the failure mechanism of snowpacks from the interaction with a blast wave.

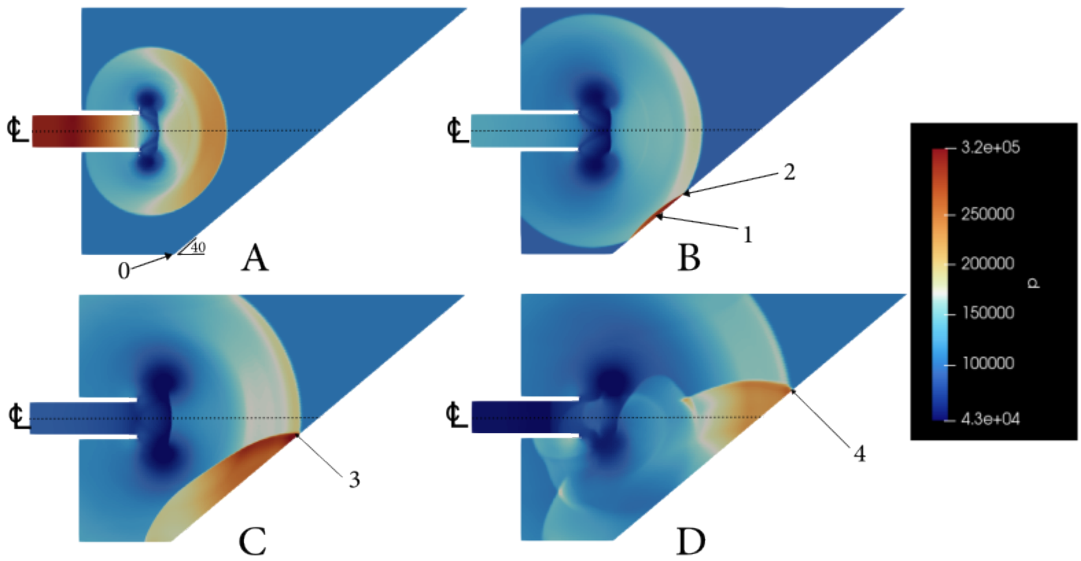

Figure 6: OpenFoam simulations conducted for a case with a surface set 40 degrees from the centerline of the tube using a high-pressure tube suddenly released. A) shows the shock expanding before it has impacted the surface (0.0018 s after release). B) shows the start of a regular reflection forming on the surface (0.0027 s after release). C) shows the regular reflection before it begins to transition to a Mach reflection (0.0037 s after release). D) shows a Mach reflection on the surface (0.0050 s after release).

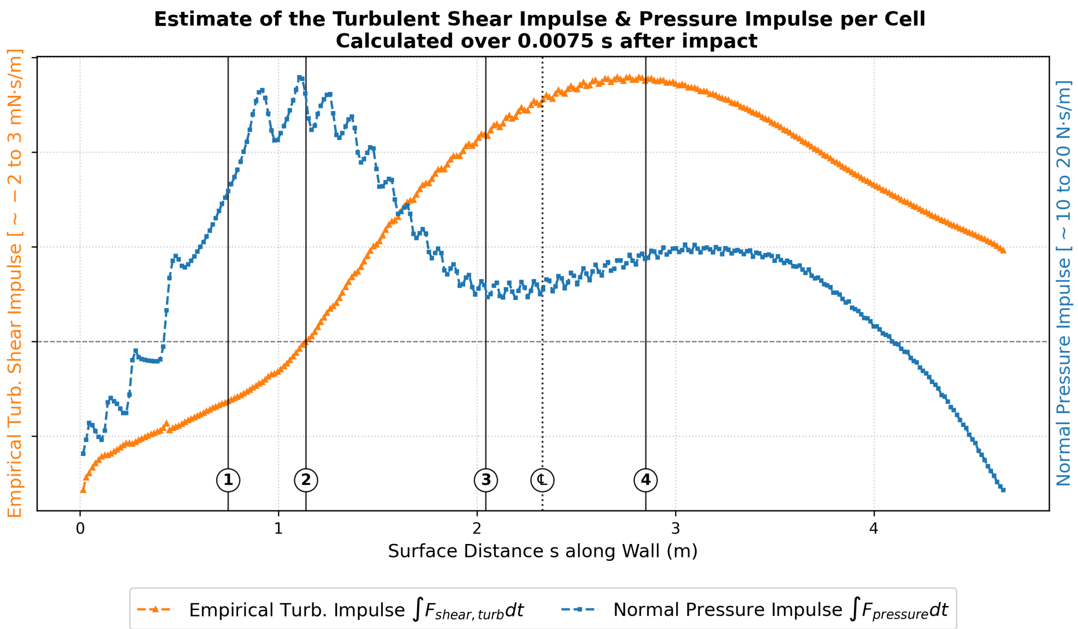

Figure 7: A plot of the estimates of normal pressure impulse calculated over 0.0075 s simulation and the estimate of the shear stress calculated from the empirical 1/7th power law.

ACKNOWLEDGEMENTS

This work was supported by the NSERC Discovery Grant ”Towards a predictive model of the cellular detonation structure in gases” (RGPIN-2025-04197) to M. Radulescu.

REFERENCES

Anand, V., Glaser, A., and Gutmark, E. (2018). Acoustic characterization of pulse detonation combustors. In: AIAA Journal 56.7, pp. 2806–2815.

Brown, R. L. (1980). An Analysis of Non-Steady Plastic Shock Waves in Snow. In: Journal of Glaciology 25.92, pp. 279–287. https://doi.org/10.3189/S0022143000010492.

Falle, S., Giddings, J., Morton, K., and Baines, M. (1993). Numerical Methods for Fluid Dynamics 4.

Friedlander, F. G. (1946). The Diffraction of Sound Pulses I. Diffraction by a Semi-Infinite Plane. In: Proceedings of the Royal Society of London. A. Mathematical and Physical Sciences 186.1006, pp. 322–344. ISSN: 0080-4630. https://doi.org/10.1098/rspa.1946.0046.

Gubler, H. (1977). Artificial Release of Avalanches by Explosives. In: Journal of Glaciology 19.81, pp. 419–429. ISSN: 0022-1430, 1727-5652. https://doi.org/10.3189/S0022143000029440.

Lachapelle, E. R. (1977). Alternate Methods for the Artificial Release of Snow Avalanches. In: Journal of Glaciology 19.81, pp. 389–397. ISSN: 0022-1430, 1727-5652. https://doi.org/10.3189/S0022143000029415.

Larson, R., Seitz, B., and Miller, D. A. (2022). Measuring Explosive Airblast of Remote Avalanche Control Systems (RACS).

Meier, B. (2024). ON TRIGGERING AVALANCHES, WHAT HAPPENS BETWEEN EXPLOSION AND RELEASE. In.

Miller, D. A., Tichota, R. G., and Adams, E. E. (2010). AN EXPLICIT NONLINEAR NUMERICAL MODEL OF EXPLOSIVE AIR BLAST ON SNOW AND IMPLICATIONS FOR AVALANCHE CONTROL. In.

Miller, D. A., Tichota, R. G., and Adams, E. E. (2011). An Explicit Numerical Model for the Study of Snow's Response to Explosive Air Blast. In: Cold Regions Science and Technology. International Snow Science Workshop 2010 Lake Tahoe 69.2, pp. 156–164. ISSN: 0165-232X. https://doi.org/10.1016/j.coldregions.2011.08.004.

Perla, R. (1976). High Explosives and Artillery in Avalanche Control. In: Proceedings of the 1976 International Snow Science Workshop, Banff, Alberta, pp. 42–49.

Seitz, B. K. (2021). "Measuring Explosive Airblast of Remote Avalanche Control Systems". Montana State University - Bozeman, College of Engineering.

Sidler, R. (2015). A Porosity-Based Biot Model for Acoustic Waves in Snow. In: Journal of Glaciology 61.228, pp. 789–798. ISSN: 0022-1430, 1727-5652. https://doi.org/10.3189/2015JoG15J040. arXiv: 1502.01284 [physics.geo-ph].

Sidler, R., Simioni, S., Dual, J., and Schweizer, J. (2016). Numerical Simulation of Wave Propagation and Snow Failure from Explosive Loading. https://doi.org/10.48550/arXiv.1603.01168. arXiv: 1603.01168 [physics.geo-ph]. URL: http://arxiv.org/abs/1603.01168 (visited on 08/28/2026). Prepublished.

Simioni, S., Dual, J., and Schweizer, J. (2017). Snowpack Response to Directed Gas Explosions on Level Ground. In: Cold Regions Science and Technology 144, pp. 73–88. ISSN: 0165232X. https://doi.org/10.1016/j.coldregions.2017.09.012.

Simioni, S. and Schweizer, J. (2018). Comparing Two Methods of Artificial Avalanche Triggering: Gas vs. Solid Explosives. In: International Snow Science Workshop Proceedings 2018, Innsbruck, Austria, pp. 158–161.